ADVANCED OPTICAL MATERIALS
www.advopticalmat.de

High-Q Plasmonic Fano Resonance for Multiband Surface-Enhanced Infrared Absorption of Molecular Vibrational Sensing

*Govind Dayal, Xin Yu Chin, Cesare Soci, and Ranjan Singh**

Realizing strong plasmon–vibration interactions between infrared-active vibrational bands and resonating plasmonic metasurfaces opens up the possibilities for ultrasensitive label-free detection of chemical and biological agents. The key prerequisites for exploiting strong plasmon–vibration interactions in practical spectroscopy are structures, which provide giant field enhancement that highly depends on the line-width and line-shape of the plasmonic resonances supported by these structures. Here, multiband surface-enhanced infrared absorption (SEIRA) of poly(methyl methacrylate) (PMMA) is demonstrated. The line-width and line-shape of the proposed plasmonic metasurface can be readily tuned to match the multiple vibrational modes of the PMMA to sense the prohibitively weak fingerprints. The tightly coupled system exhibits mode splitting in the optical spectrum resulting in new hybrid plasmon–phonon modes of PMMA. Such a strong interaction of high-Q Fano resonances to multiple phonon modes in ultrathin film analytes over a broadband spectral range could be step forward towards ultrasensitive sensing of biological and chemical molecules.

1. Introduction

Infrared (IR) spectroscopy is a powerful tool that provides the most definitive approach to identify bond types, structures, and functional groups present in organic and inorganic compounds.[1] When IR radiation is absorbed by a molecule, it causes vibrational and rotational modes. Since vibrational energy transitions are quantized such modes absorb a photon with a frequency equal to the natural vibrational frequency of the corresponding molecular bonds. Infrared spectroscopy investigates vibrational modes associated with specific molecular bonds and chemical functional groups, that are unique to each specific compound and contains information about chemical composition and structure, e.g., OH, NH, C=O, C=C, etc., by measuring the absorption in the infrared spectral region. The experimentally obtained infrared spectra are then compared with widely established databases that enable a rapid identification of materials which is a common procedure in analytical chemistry, biology and medicine. Most organic functional group absorption occurs in the mid-IR range, between 2.5 and 25 μm (4000 and 400 cm^{-1}), respectively. The absorption of infrared light can be characterized by the Bouger Lambert–Beer law. According to Bouger Lambert–Beer law, the amount of light absorbed is proportional to the extinction coefficient (α),which depends on the nature and state of the substance, the wavelength (λ) of the radiation, and the absorption path length "*d*," and is mathematically expressed as $I(d) = I_0 e^{-\alpha(\lambda)d}$, where I_0 is the intensity of the beam entering a layer of matter. From this expression, it can explicitly be seen that the absorption decreases exponentially with decreasing thickness of the material and thus it becomes extremely challenging to detect/sense the absorption of the material which is only a few layers thick. In the extreme case of a monolayer, the absorption signal becomes prohibitively weak.

In 1980, Hartstein et al. reported the first intensification of infrared-active vibrational modes of organic thin film on a silicon substrate by evaporating a thin metal film (Ag and Au) on to the organic film.[2] The phenomenon of surface-enhanced infrared absorption (SEIRA) is explained as the coupling between the vibrational modes of the molecules and the enhanced optical fields near the surface of the particles under the assumption that the film is not continuous but consists of metal islands smaller than the wavelength of light.[3–7] Thin metal films consisting of metal islands smaller than the wavelength of light exhibit plasmonic resonances because of the coherent oscillation of free electrons in the metal islands. This resonant excitation and the related near-field enhancement is known as localized surface plasmon resonance. The field enhancement depends largely on the morphology of the metal surface. For metal films consisting of randomly distributed metal islands, the overall response of individual metal island resonators with various sizes results in a broadband resonance with a poor quality factor (*Q*).

Dr. G. Dayal, X. Y. Chin, Prof. C. Soci, Prof. R. Singh
Division of Physics and Applied Physics
School of Physical and Mathematical Sciences
Nanyang Technological University
21 Nanyang Link, Singapore 637371
E-mail: ranjans@ntu.edu.sg
Dr. G. Dayal, X. Y. Chin, Prof. C. Soci, Prof. R. Singh
Center for Disruptive Photonic Technologies
The Photonics Institute
Nanyang Technological University
50 Nanyang Avenue, Singapore 639798

DOI: 10.1002/adom.201600559

With the advances in nanofabrication techniques, it has now become possible to fabricate the metallic structures with geometrical precision down to few nanometers. These well-defined nanostructures can have the sharp spectral signatures that can be tuned with geometrical shape and dielectric constant of the nanostructures and also with the illumination properties (polarization, wavelength) to match the vibrational modes of a particular molecule.[8–14] Metallic nanoparticles supporting localized surface plasmons have received a great deal of attention for their unique ability to convert far-field radiation into near-field hotspots which provides an ideal platform for achieving enhanced optical interaction at the nanoscale. In metallic nanoparticles, the optical response is mainly governed by the excitation of localized surface plasmons, the collective oscillation of the surface charge density at the particle following the electromagnetic modes imposed by the geometrical boundary conditions.[15] In the case of light scattering by plasmonic nanostructures, the dipole resonance plays the role of a super-radiant (bright) mode while the higher-order multipoles (e.g., quadruple, octupole, etc.) play the role of sub-radiant (dark) modes. Super-radiant plasmon mode possesses finite dipole moments and are spectrally broadened due to radiative damping. The super-radiant resonance strongly couples to the incident light. Sub-radiant plasmon modes, on the other hand, are weakly damped, spectrally narrow, and do not couple efficiently to the incident light. Recently, it has been demonstrated that a sub-radiant mode can be excited indirectly through the coupling with a super-radiant mode by breaking the structural symmetry of the plasmonic nanostructure. The asymmetry results in interaction and mixing of super-radiant and higher order modes that give rise to new hybridized plasmon modes. One of the most interesting phenomena arising from the hybridization is the Fano resonance effect, which could result from the interference between super-radiant modes and sub-radiant modes.[16–18] Fano resonances are characterized by a steeper dispersion than conventional Lorentzian resonances which makes them promising for local refractive index sensing applications to confine light more efficiently and for surface enhanced infrared absorption.[19,20]

The infrared-active vibrational modes of a chemical or biological compound can be classified as strong, medium, or weak, depending on their relative intensities in the infrared absorption spectrum. In most of the previous studies on SEIRA,[21–23] the plasmonic resonances were tailored to match the strongest vibrational mode of the compound, e.g., C=O bond of poly(methyl methacrylate), PMMA, that has the strongest dip at around 5.773 μm (1732 cm^{-1}) range. However, identifying a single functional group is insufficient as a particular functional group may be present in many other compounds too. For instance, the C=O functional group, which is most often coupled to plasmonic resonance to enhance the vibrational signal of poly(methyl methacrylate), is also present in several other compounds such as ethyl butyrate (@ 1738 cm^{-1}), methyl methacrylate (@ 1725 cm^{-1}), methyl benzoate (@1724 cm^{-1}), etc. Hence, in order to get a conclusive finger print of the molecular structure of a compound, one needs to identify the vibrational modes associated with more than one functional group. In SEIRA, this can be achieved by exploiting the local field enhancement of metasurfaces that can be tuned to cover the entire vibrational absorption band of interest. A broad plasmonic resonance can cover many vibrational modes but at the expense of local field enhancements which depends on the quality factor (Q) of the resonances. Thus, the plasmon-vibrational mode coupling, which increases the sensitivity, is drastically reduced and the weak vibrational modes with small dipole moments cannot be identified. One way to overcome this fundamental deficit involves engineering of multispectral plasmonic metasurfaces that are designed to match the vibrational modes of the compound. In order to achieve high enhancement levels, such plasmonic resonances should have higher Q-factors.

In this letter, we propose and demonstrate a novel multiresonant plasmonic metasurface whose line-width and line-shape of the super-radiant and sub-radiant modes can be tailored to match specific vibrational modes. As a proof-of-concept, we demonstrate the detection of molecular fingerprints of a thin poly(methyl methacrylate), PMMA film coated on top of the tunable multiresonant plasmonic metasurface. PMMA polymer has several well-characterized IR absorption bands in the 5.773 μm (1732 cm^{-1}), 7.169–6.897 μm (1395–1450 cm^{-1}), 7.963–9.615 μm (1260–1040 cm^{-1}), 11.36–10.41 μm (880–960 cm^{-1}) range that are ascribed to the CH stretching vibration, CO double bond stretching vibration, CH_3 and CH_2 deformation vibration, COC single bond stretching vibration and COC single bond deformation vibration, respectively. Here, we target the absorption bands from 10.0 to 4.0 μm (1000 to 2500 cm^{-1}) spectral range. Our proposed metasurface design consists of multiple concentric annular apertures, where the outermost annular aperture overlaps with a rectangular aperture. Multiple concentric annular apertures are used in this study to achieve multiband spectral response at desired spectral bands. The optical properties of sub-wavelength annular aperture arrays have been intensively studied subject due to their enhanced transmission properties. Their large transmission is due to coupling between the propagating surface plasmon mode and the guided mode (TE_{11}-like mode) propagating inside each cavity.[24] The cutoff wavelength for the dominant TE_{11} mode occurs at a wavelength approximately equal to $\pi(R_{n,o} + R_{n,i})$, where $R_{n,i}$ and $R_{n,o}$ indicates the inner and outer radius of the nth annular aperture, respectively.[25–27] In our case, the geometrical dimensions of the outermost annular aperture and the rectangular aperture are prudently chosen in such a way that the spectral response of the individual resonator overlaps. Spectral and spatial overlaps of the two resonators gives rise to the high-Q Fano resonances that can be tuned through the polarization of the incident radiation.

2. Results and Discussion

Figure 1a illustrates the schematic view of the proposed metasurface design consisting of two concentric annular apertures where the outermost annular aperture overlaps with a rectangular aperture. In this figure, $R_{n,o}$ indicates the outer radius of the n^{th} annular aperture. The aperture width has been kept constant at 100 nm for all the apertures. Figure 1b–d shows the top view of scanning electron microscope (SEM) picture of the unit cell of the fabricated metasurfaces consisting of one, two, and

Adv. Optical Mater. 2016,
DOI: 10.1002/adom.201600559

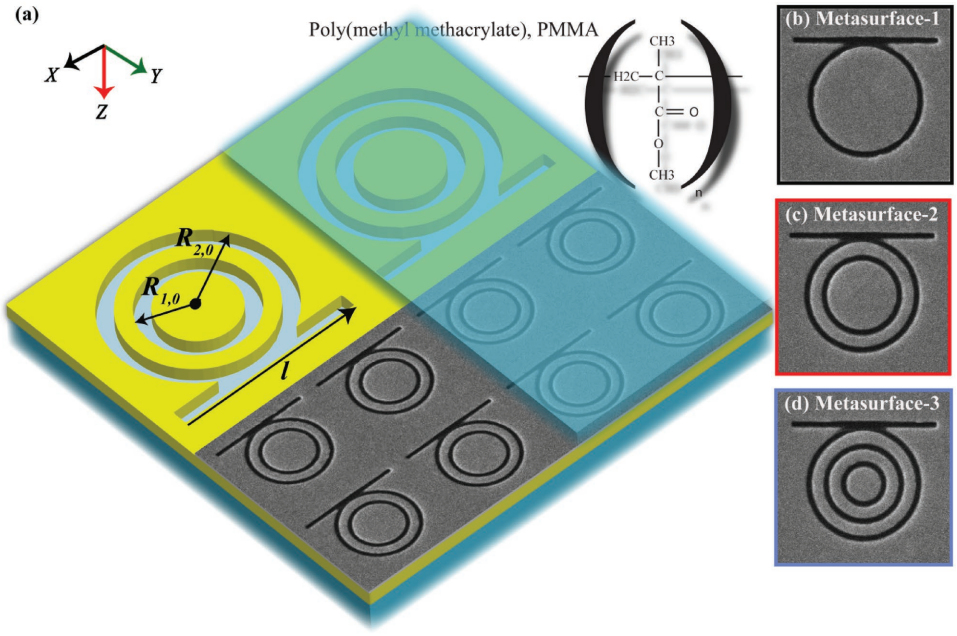

Figure 1. a) Schematic diagram of the proposed metasurface consisting of concentric annular and rectangular apertures. The specific geometrical parameters of the unit cell are $R_{2,0} = 1$ µm, $R_{1,0} = 0.8$ µm, and $l = 2.5$ µm. b–d) The SEM images of the unit cell of the fabricated samples are shown. A 50 nm thin layer of poly(methyl methacrylate), PMMA, is spin coated on top of the metasurface.

three concentric apertures arrays. All the structures are milled in a 100 nm thick Au film deposited on a quartz substrate using focused ion beam (FIB, Helios Nanolab 600) milling. The three concentric ring apertures have outer radii of 1000, 800, 600 nm, and an edge-to-edge gap between them is d = 200 nm. The length and width of the rectangular apertures are 1200 and 100 nm, respectively. The total size of each metasurface array is 50 µm × 50 µm.

The measured and simulated reflectance spectra for different polarizations are revealed in **Figure 2** for the structures shown in Figure 1b–d. The polarization of the incident electric field is defined with respect to the length of the rectangular aperture, i.e., *x*-polarization for *E*-field polarized along the length of the aperture and *y*-polarization for *E*-field polarized perpendicular to the length of the rectangular aperture. Figure 2a,b illustrate the experimentally measured and numerically simulated spectra for *x*-polarization. The measured reflection spectrum (black curve) for the metasurface-1 shows a broad dip at 7.47 µm and two sharp Fano resonance dips at 5.72 and 4.61 µm, respectively. The spectral response of arrays of single annular aperture overlapping with rectangular aperture has been investigated in our previous communication.[28,29] We find that the dip in the reflection spectrum at 7.47 µm is due to the dipole mode (m = 2) of the annular aperture and the Fano dips at 5.72 and 4.61 µm are due to the interference of the azimuthal quadrupolar mode (m = 4) of the annular aperture with the dipolar and quadrupolar modes of the rectangular aperture. The measured reflection spectrum (red curve in Figure 2a) of metasurface-2 consisting of two concentric annular apertures show two broad dips at 7.67 and 5.2 µm, and an asymmetric line-shape Fano resonance dip at 4.65 µm. Numerically calculated electric field distribution plots at the corresponding dips in the simulated spectrum of metasurface-2 reveals the underlying physics of the plasmonic resonances.

The electric field distribution shown in **Figure 3**a,b, at the broad resonances located at 7.67 and 5.2 µm originate from the resonant excitation of the azimuthal dipole modes (m = 2) in the outer and inner annular apertures, respectively. The sharp asymmetric line-shape dip at 4.65 µm arising due to the spectral overlap of the azimuthal quadrupolar mode (m = 4) of the outer annular aperture with the dipolar mode of the rectangular aperture and the azimuthal dipolar mode of the inner annular aperture can clearly be seen in the electric field distribution shown in Figure 3c. Compared to the reflection spectrum of metasurface-1, we find that the spectral width of the dipole resonance of the outer annular aperture is considerably narrowed down due to the presence of the inner aperture. The spectral narrowing of the plasmonic resonances can be understood in terms of the interaction and hybridization of plasmon modes of the inner and outer apertures. As shown in Figure 3a, the dipolar charge distribution of the inner and outer annular apertures, at the dipole resonance frequency of outer aperture, are out of phase. The hybridization of these two out of phase plasmon modes results in the reduction of the net dipole moment which in turn reduces the radiative loss of the dipolar plasmon mode of the outer aperture. This spectral narrowing, which will have a direct consequence on the electric field enhancement, is extremely useful in the amplification of the vibrational signal. We found that the spectral width can be further narrowed down by increasing the radius of the inner annular aperture which reduces the edge-to-edge gap between the outer and inner apertures. The metasurface-3 with three concentric annular apertures shows approximately the same optical behavior as for the metasurface-2 but with a much narrower dipole resonance of

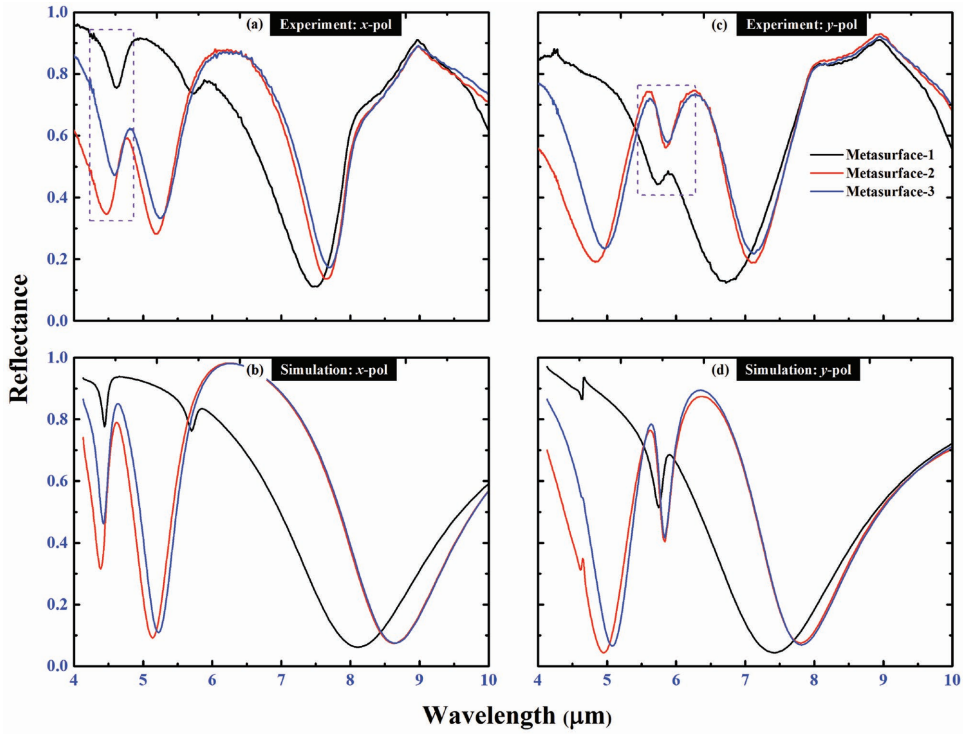

Figure 2. Measured (top panel) and simulated (bottom panel) reflection spectra of the three different metasurfaces. a,b) The incident electric field is polarized in the *x*-direction (parallel to the long axis of the rectangle). c,d) The field is polarized in the *y*-direction (perpendicular to the long axis of the rectangle).

the intermediate annular aperture and Fano resonance (blue curve in Figure 2a). In the case of metasurface-3, the line-width of the dipole resonance of the outer aperture is also narrowed in comparison to the line-width of the dipole resonance of the annular aperture of the metasurface-1 due to the interaction between the outer and intermediate apertures. Furthermore, from the graph of Figure 2a, we note that the line-widths of the dipolar plasmon mode of the intermediate aperture and

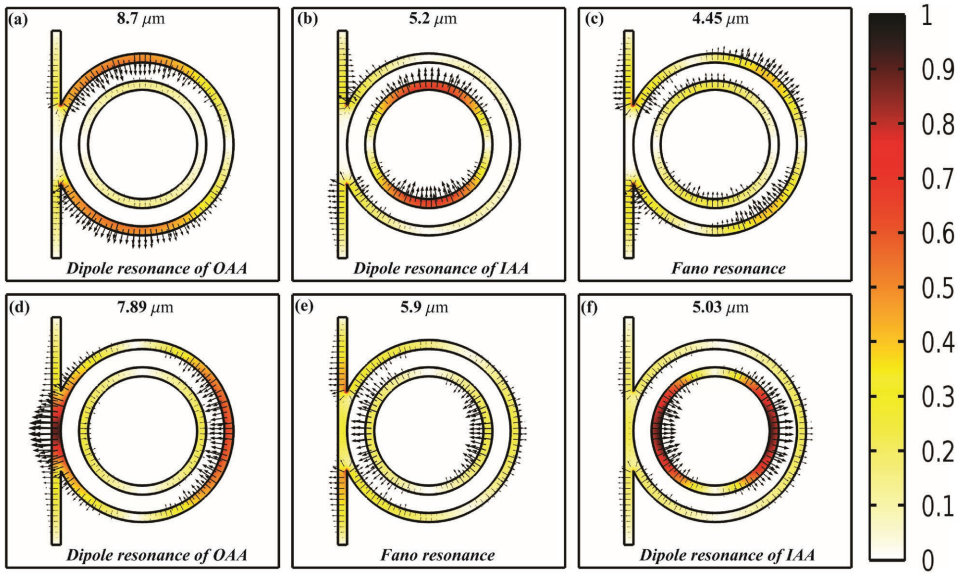

Figure 3. Simulated electric field distribution (black arrows) in the *x*–*y* plane of the metasurface-2 at respective resonance dip positions in the reflection spectra for the *x*-polarization (top panels; (a–c)) and the *y*-polarization (bottom panels; (d–f)) The arrows represent the vectors of electric field and the color contour plot indicates the electric field norm.

Adv. Optical Mater. **2016**,
DOI: 10.1002/adom.201600559

the Fano resonance of metasurface-3 of the intermediate aperture undergoes resonance line narrowing due to the interaction between the intermediate and innermost apertures. The interaction between outer and innermost apertures of metasurface-3 is negligibly small due to the wide spectral gap between the dipolar resonances of the outermost and innermost resonators. The slight mismatch between the experimental and numerical simulation is due to the assumption of non-dispersive dielectric constant (n = 1.45) of SiO_2 in the numerical simulation which is actually dispersive in the 6–10 μm range.

Next, we present the reflection spectra of three different metasurfaces for the *y*-polarized light. The measured reflection spectrum (black curve in Figure 2c) for the metasurface-1 shows a broad dip at 6.67 μm and a sharp Fano resonance dip at 5.74 μm. The resonance dip in the reflection spectrum at 6.67 μm is due to the collective excitation of the azimuthal dipole mode (m = 2) in the annular aperture and the asymmetric line-shape dip at 5.74 μm is due to the excitation of the Fano resonance resulting from the spectral overlap of the azimuthal quadrupolar mode (m = 4) of the annular aperture with the dipolar and quadrupolar mode of the rectangular aperture. In the case of two concentric annular apertures, the measured reflection spectrum (red curve in Figure 2c) shows two broad dips at 7.1 and 4.82 μm and a sharp Fano resonance dip at 5.86 μm. The simulated electric field distributions at resonance frequencies of 7.1 and 4.82 μm in the corresponding simulated spectrum reveal the excitation of the dipole modes (m = 2) in the outer and inner annular apertures, respectively, and the sharp symmetric line-shape dip at 5.86 μm is due to the formation of the Fano resonances resulting from the spectral overlap of the azimuthal quadrupolar mode (m = 4) of the outer annular aperture with the dipolar of the rectangular aperture and dipolar of the inner annular aperture. It is interesting to note that line-shape of the Fano resonance, which is conventionally characterized by an asymmetric line-shape dispersion in the optical scattering '$S(\omega)$', has now become symmetric due to the presence of another background created by dipolar resonance of the inner annular aperture. Fano explained the asymmetric shape of spectral lines based on the superposition between two scattering channels involving a continuum and a discrete state with an asymmetric line-shape given by

$$S(\omega) = (\mathrm{F}\gamma + \omega - \omega_0)^2/(\omega - \omega_0)^2 + \gamma^2 \quad (1)$$

where ω_0 and γ denote the spectral resonance position and width of the resonance, respectively; F is the so-called Fano parameter, which describes the degree of asymmetry. In our case, the Fano resonance arises due to spectral overlap of a sub-radiant mode with two super-radiant modes that are judicially engineered to be on the red and blue side of the Fano dip to control the parameter F, which describes the degree of asymmetry of the Fano resonance. To elucidate this concept in greater detail, we carried out the numerical simulation of metasurface-2 with varying the radius of the inner aperture while keeping the radius of outer aperture constant. Varying the radius of the inner aperture would significantly modify the shape of the Fano resonances as the interaction between the outer and inner aperture would change. The simulated spectra of metasurface-2 with outer radii of the inner and outer aperture of 0.7 and 1 μm, respectively, for the *y*-polarization shows a slightly asymmetric Fano resonance at 5.83 μm as shown in Figure 3 of the Supporting Information. As the outer radius of the inner aperture decreases to 0.65 μm, we observe a perfectly symmetric Fano resonance at 5.83 μm. When the inner radius of the inner aperture is further reduced to 0.625 μm, the shape of Fano resonance becomes asymmetric. From the simulated reflection spectra for *x*-polarization, we find that as the radius of the inner aperture decreases, dipole resonance red-shifts while the Fano resonance shifts toward the blue. This opposite shifts in the dipole and Fano resonance sharpens the steepness of the Fano resonance as plotted in Figure 2 of the Supporting Information. Thus, the line-shape of the Fano resonances from asymmetric to a near symmetric shape can be controlled with extreme precision through slight variation in the metasurface structural design.

To perform the surface enhanced infrared absorption spectroscopy of PMMA, we spin coated a 50 nm thin layer of PMMA on top of the fabricated metasurfaces as shown in Figure 1b–d. The plots in **Figure 4** show the FTIR spectra of the 50 nm thin PMMA coated plasmonic metasurfaces for two orthogonal polarizations. A reference measurement of PMMA on a quartz substrate is presented in green. On the reflection spectra of PMMA coated metasurfaces, the following characteristic absorption bands appear: the dips representing the stretching vibration of the C—O—C and C—H at 7.69–9.09 μm (1300–1100 cm^{-1}); the dips representing the bending vibration of $-CH_2$ and $-CH_3$ groups at 6.934 μm (1442 cm^{-1}) and 7.204 μm (1388 cm^{-1}); the stretching dip of C=O in carbonyl groups at 5.773 μm (1732 cm^{-1}), respectively. These features are not detectable in the reflection spectrum of the reference and can only be identified in the amplified absorption spectra arising from the plasmon-vibration coupling in the PMMA coated metasurface system. The resulting enhancement of the absorption signals of PMMA fingerprints is a manifestation of strong light-matter interaction due to a strong plasmon–phonon coupling. The enhancement in the absorption amplitude of molecular vibration is mainly determined by the local field enhancement and consequently the enhanced local density of states of the IR photons at the resonant dips. In the electric dipole approximation, the coupling operator $H = -p_m \bullet E_{loc,}$ where p_m is the component of the molecular dipole in the direction of the electric field E, and E_{loc} is the local electric field near the metasurface. Therefore, to enhance the absorption amplitude of molecular vibration of a given functional group that has to be seen with maximum vibrational infrared absorption intensity, the spectral position of plasmonic resonances, where the near-field enhancement is maximum, must align with the resonance frequency of the absorption band of the functional group. As shown in Figure 4a, the dipolar resonances of the outer and inner annular apertures of the metasurface-2 for the *x*-polarization incidence are tuned to spectrally overlap with the stretching vibration of the C—O—C and C—H functional groups at 7.69–9.09 μm (1300–1100 cm^{-1}) and the stretching dip of C=O in carbonyl groups at 5.77 μm (1732 cm^{-1}), respectively (red curve in Figure 4a). The absorption bands of the stretching vibration of the C—O—C and C—H functional groups that are matched with the metasurface resonance dips show maximum enhancement in the absorption amplitude because the absorption scales with the intensity of the local field created

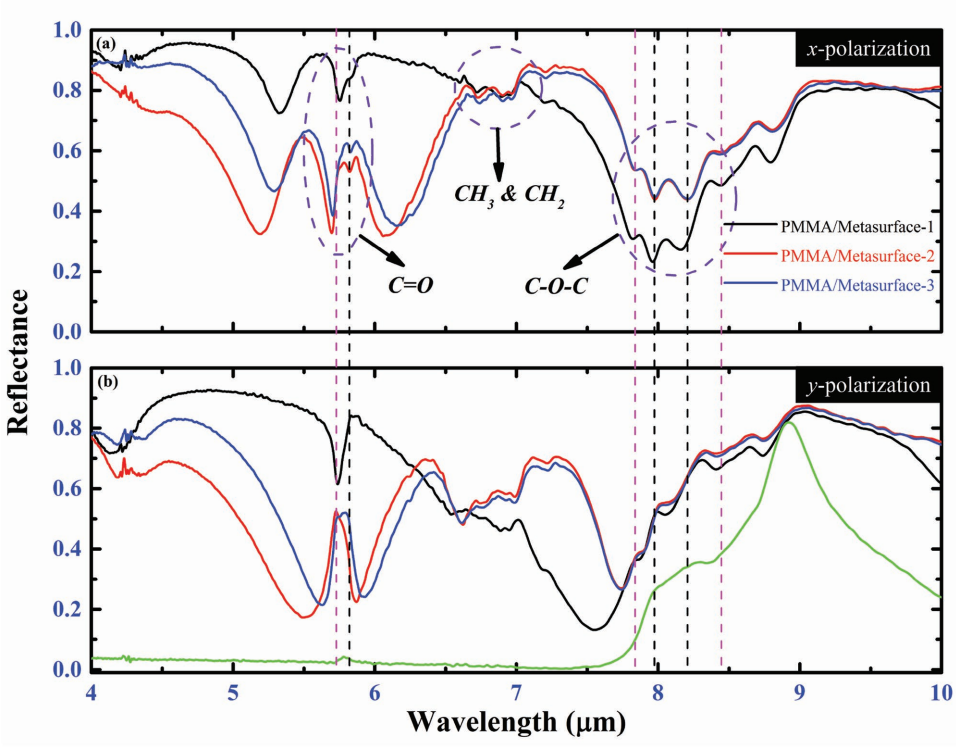

Figure 4. SEIRA spectroscopy of PMMA coated on the metasurfaces. Reflectance spectra of the three metasurfaces for *x* (top) and *y* (bottom) polarizations after the coating of a 50 nm thick PMMA film. a) Characteristic vibrational stretching modes of the C—O—C at 8.038 μm (1244 cm^{-1}) strongly coupled with the plasmonic resonance resulting in two new hybrid plasmon–phonon modes that are visible in the spectra as indicated by the dashed black lines. b) When the plasmon resonance is detuned for *y*-polarization incidence, the splitting disappears.

at the molecular position. The vibrational resonance mode of PMMA molecules at 8.038 μm (1244 cm^{-1}) which corresponds to the C—O—C strongly couples with the enhanced near-field of plasmonic resonance, resulting in two new hybrid plasmon–phonon modes (black dotted lines) that produces a unique dual resonance feature (at 7.97 and 8.27 μm) in the reflectance spectrum.[30,31] We observed that the spectral gap of the two minima that resulted from the interaction between the metasurface with increasing *Q*-factor broadens the gap between the two hybrid modes. When the plasmonic resonances are detuned by switching the polarization of incident light from *x*- to *y*-direction, the absorption bands at 7.67–9.09 μm (1300–1100 cm^{-1}) fall on the red side of the plasmonic resonance dip due to blue shifting of plasmonic resonances and plasmon-vibration interaction changes from strong coupling to weak coupling regime. Due to this weak coupling, the amplitude of the vibrational absorption mode gets attenuated and the mode-splitting behavior of the plasmon-vibration coupled resonances disappears as shown in Figure 4b. It is worth noticing that the absorption amplitude of the C—O—C and C—H functional groups at 7.67–9.09 μm for metasurface-2 is comparable to metasurface-1 despite of the lower amplitude of the plasmonic resonances as shown in Figure 4a. The reduction in amplitude of the plasmonic resonance is compensated by the higher *Q* factor of the dipole resonance of the metasurface-2. Next, we consider the plasmonic interaction of C=O in carbonyl group at 5.77 μm (1732 cm^{-1}) which is the largest for all metasurfaces because of its intrinsic large dipole moment. One interesting observation to note here is the explicit evidence of another vibrational band at 5.82 μm (1718 cm^{-1}) in the reflection spectra of the metasurface-2 and metasurface-3, respectively, as shown in Figure 4a. This remarkably enhanced contrast in the absorption spectrum is enabled by steep dispersion of the Fano resonance profile which is engineered to match the vibrational mode of the C=O functional groups. Such a clear resolution of the strong and weak vibrational modes has not been observed before.

From the experimentally observed spectra, we also find that the spectral positions of these plasmonically coupled vibrational bands are observed to be slightly off from their original values due to light-matter interaction between the localized IR photons and the molecular vibrational modes. We note that this spectral shift is strongly dependent on the nature of the plasmonic resonances and is different for metasurfaces consisting of the single, double, and triple concentric apertures. It is furthermore noted that line- shape of the absorption bands of different functional groups is distorted from its normal Lorentzian shape exhibiting an asymmetric Fano profile-like shape, which is due to spectral overlap of the narrow band vibrational modes with a comparatively broad background resonance supported by the plasmonic metasurface. The red-shifting of plasmonic resonances in the reflection dips of the PMMA coated metasurfaces is due to the effective increase in the background dielectric constant which can be determined from the film thickness and the

Adv. Optical Mater. **2016**,
DOI: 10.1002/adom.201600559

refractive index of the film. Thus, increasing or decreasing the analyte thickness would shift the plasmonic resonance which will detune the coupling between the plasmonic resonance and a chosen vibrational mode. This has been a major drawback of the plasmonic metasurface with fixed spectral response. In our metasurfaces, the plasmonic resonances can be tuned through the polarization of the incident light to match the chosen vibrational mode for a range of analyte thicknesses.

In summary, we have demonstrated a novel plasmonic metasurface that can support both the super-radiant and sub-radiant plasmonic modes in the mid-infrared range. The superposition of super-radiant mode and sub-radiant mode produces high-Q Fano resonances in the reflection spectrum of the metasurfaces. We showed that the line-width, line-shape, and the spectral position of the super-radiant modes and Fano resonant modes can be controlled. We also present a new method to control the asymmetry parameter of the Fano resonances. Tunable multispectral response of proposed metasurface makes it a promising candidate for the studying light matter interaction, especially SEIRA, which could enable close monitoring of several characteristic molecular vibrational modes simultaneously. To demonstrate this, we performed the multiband surface-enhanced infrared spectroscopy of PMMA. The precisely engineered plasmonic resonances of the proposed metasurface can be readily tuned to match the multiple vibrational modes of the PMMA spread throughout the mid-infrared range. The observation of surface enhanced infrared absorption confirms that light–matter interaction can significantly modify the vibrational frequency of chemical bonds. The plasmon-vibration mode coupling is shown to be strongly dependent on the line-width and line-shape of the plasmonic resonances. We find that asymmetric shape plasmonic Fano resonances with steeper dispersion than the plasmonic dipole modes can reveal much finer details about the infrared fingerprints enabling a route towards highly accurate chemical and biomolecular sensing. We also demonstrate that the plasmon-vibration interactions can be switched from strong to weak coupling regime by switching the polarization of the incident light.

3. Experimental Section

Fabrication: A thin 80 nm gold film is deposited onto a quartz substrate using thermal evaporation method (evaporation rate 0.5 Å s^{-1}). The plasmonic metasurfaces consisting of annular and rectangular apertures array are then fabricated via focused ion beam milling, carried out in a FEI Helios Nanolab 600 Dual Beam microscope system with the focused beam of gallium ions of the current of 24 pA and the energy of 30 eV. Each sample has a 50 µm × 50 µm pattern area.

PMMA Layer Preparation: A thin layer of poly(methyl methacrylate) PMMA (950-A2, 2% solid content in anisole, Michrochem) is spin-coated on top of the metasurfaces at 4000 rpm for 60 s.

Simulation: The full-field electromagnetic simulations are carried out using a finite element method-based software package, Comsol Multiphysics. The optical properties of the metal in the simulation are characterized by a complex-frequency-dependent dielectric permittivity described by Drude free electron model $\varepsilon(\omega) = \varepsilon_\infty - \omega_p^2/(\omega^2 + i*\omega*\gamma)$ with the plasma frequency $\omega_p = 2\pi*2175$ THz and the collision frequency $\gamma = 2\pi*15$ THz. The quartz substrate is characterized by a real-frequency-independent dielectric constant $n_d = 1.45$. In the simulation, the Floquet periodic boundary conditions are applied for the transverse boundaries of the unit cell to replicate an infinite planar array of the unit cell. Port boundary conditions are used, perpendicular to the z-axis, to excite a plane wave from the top of the structure with a power of 1 W. The reflection ($R(\lambda)$) spectrum was calculated from S-parameters. Perfectly matched layers (PMLs) are applied along the propagation direction (perpendicular to the planar metasurface) to avoid multiple reflections due to geometry truncation.

FTIR Measurements: The reflection spectra of the fabricated samples before and after PMMA coating are recorded using a Fourier transform infrared (FTIR) spectrometer (Bruker Vertex 80v) equipped with a confocal microscope (Hyperion 1000) with a liquid-nitrogen-cooled mercury cadmium telluride (MCT) detector. Reflected signals are collected with a 36× confocal objective with 0.5 NA. A ZnSe polarizer is used to polarize the incident electromagnetic field. All the spectra are recorded with a resolution of 4 cm^{-1} and 100 scans. All measurements are normalized with respect to the reflectance from a plain gold mirror.

Supporting Information

Supporting Information is available from the Wiley Online Library or from the author.

Acknowledgements

The authors acknowledge research funding support from NTU startup Grant No. M4081282, Singapore MOE Grant Nos. M4011362, M4011534, MOE2011-T3-1-005, and MOE2015-T2-2-103.

Received: July 14, 2016
Revised: September 12, 2016
Published online:

[1] R. Aroca, *Surface-Enhanced Vibrational Spectroscopy*, John Wiley & Sons, Chichester, UK **2006**.
[2] A. Hartstein, J. R. Kirtly, J. C. Tsang, *Phys. Rev. Lett.* **1980**, *45*, 201.
[3] M. Osawa, K. Ataka, K. Yoshii, Y. Nishikawa, *Appl. Spectrosc.* **1993**, *47*, 1497.
[4] E. Johnson, R. Aroca, *J. Phys. Chem.* **1995**, *99*, 9325.
[5] A. Roseler, E.-H. Korte, *Appl. Spectrosc.* **1997**, *51*, 902.
[6] G. T. Merklin, P. R. Griffiths, *J. Phys. Chem.* **1997**, *101*, 5810.
[7] G. T. Merklin, P. R. Griffiths, *Langmuir* **1997**, *13*, 6159.
[8] F. Neubrech, A. Pucci, T. W. Cornelius, S. Karim, A. GarcáEtxarri, J. Aizpurua, *Phys. Rev. Lett.* **2008**, *101*, 157403.
[9] L. V. Brown, K. Zhao, N. King, H. Sobhani, P. Nordlander, N. J. Halas, *Am. Chem. Soc.* **2013**, *135*, 3688.
[10] J. M. Hoffmann, H. Janssen, D. N. Chigrin, T. Taubner, *Opt. Express* **2014**, *22*, 14425.
[11] C. Huck, F. Neubrech, J. Vogt, A. Toma, D. Gerbert, J. Katzmann, T. Härtling, A. Pucci, *ACS Nano* **2014**, *8*, 4908.
[12] H. Aouani, H. Šípová, M. Rahmani, M. Navarro-Cia, K. Hegnerová, J. Homola, M. Hong, S. A. Maier, *ACS Nano* **2013**, *7*, 669.
[13] E. Cubukcu, S. Zhang, Y. S. Park, G. Bartal, X. Zhang, *Appl. Phys. Lett.* **2009**, *95*, 043113.
[14] K. Chen, R. Adato, H. Altug, *ACS Nano* **2012**, *6*, 7998.
[15] S. Enoch, N. Bonod, *Plasmonics: From Basics to Advanced Topics*, Springer, Berlin, Germany **2012**.
[16] B. Luk'yanchuk, N. I. Zheludev, S. A. Maier, N. J. Halas, P. Nordlander, H. Giessen, C. T. Chong, *Nat. Mater.* **2010**, *9*, 707.
[17] A. E. Miroshnichenko, S. Flach, Y. S. Kivshar, *Rev. Mod. Phys.* **2010**, *82*, 2257.

[18] V. A. Fedotov, M. Rose, S. L. Prosvirnin, N. Papasimakis, N. I. Zheludev, *Phys. Rev. Lett.* **2007**, *99*, 147401.
[19] R. Singh, W. Cao, I. Al-Naib, L. Cong, W. Withayachumnankul, W. Zhange, *Appl. Phys. Lett.* **2014**, *105*, 171101.
[20] C. Wu, A. B. Khanikaev, R. Adato, N. Arju, A. A. Yanik, H. Altug, G. Shvets, *Nat. Mater.* **2012**, *11*, 69.
[21] C. Huck, J. Vogt, M. Sendner, D. Hengstler, F. Neubrech, A. Pucci, *ACS Photonics* **2015**, *2*, 1489.
[22] T. G. Mayerhöfer, R. Knipper, U. Hübner, D. Cialla-May, K. Weber, H.-G. Meyer, J. Popp, *ACS Photonics* **2015**, *2*, 1567.
[23] T. Neuman, C. Huck, J. Vogt, F. Neubrech, R. Hillenbrand, J. Aizpurua, A. Pucci, *J. Phys. Chem. C* **2015**, *119*, 26652.
[24] F. I. Baida, A. Belkhir, D. Van Labeke, O. Lamrous, *Phys. Rev. B* **2006**, *74*, 205419.
[25] W. Fan, S. Zhang, B. Minhas, K. J. Malloy, S. R. J. Brueck, *Phys. Rev. Lett.* **2005**, *94*, 033902.
[26] B. Moreau, G. Granet, F. I. Baida, D. Van Labeke, *Opt. Express* **2003**, *11*, 1131.
[27] D. Yoo, N.-C. Nguyen, L. Martin-Moreno, D. A. Mohr, S. Carretero-Palacios, J. Shaver, J. Peraire, T. W. Ebbesen, S. Oh, *Nano Lett.* **2016**, *16*, 2040.
[28] G. Dayal, X. Y. Chin, C. Soci, R. Singh, *Adv. Opt. Mater.* **2016**, *4*, 1295.
[29] G. Dayal, X. Y. Chin, C. Soci, R. Singh, *Adv. Opt. Mater.* **2016**, DOI: 10.1002/adom.201600417.
[30] L. Novotny, *Am. J. Phys.* **2010**, *78*, 1199.
[31] C. Shalabney, J. George, J. A. Hutchison, G. Pupillo, C. Genet, T. W. Ebbesen, *Nat. Commun.* **2015**, *6*, 5981.